Shifted-excitation Raman difference spectroscopy for *in vitro* and *in vivo* biological samples analysis

Mário Augusto da Silva Martins,[1] Dayana Gonçalves Ribeiro,[1] Edson Aparecido Pereira dos Santos,[1] Airton Abrahão Martin,[1] Adriana Fontes,[2] and Herculano da Silva Martinho[3,*]

[1]*Instituto de Pesquisa e Desenvolvimento, UNIVAP, 12244-050, São José dos Campos, São Paulo, Brazil*
[2]*Departamento de Biofísica e Radiobiologia do Centro de Ciências Biológicas, Universidade Federal de Pernambuco, 50670-901, Recife, PE, Brazil*
[3]*Centro de Ciências Naturais e Humanas, Universidade Federal do ABC, Rua Santa Adélia, 166, 09210-170, Santo André, SP, Brazil*
herculano.martinho@ufabc.edu.br

Abstract: The contamination of the Raman scattering signal with luminescence is a well-known problem when dealing with biological media excited by visible light. The viability of the shifted-excitation Raman difference spectroscopy (SERDS) technique for luminescence suppression on Raman spectra of biological samples was studied in this work. A tunable Lithrow-configuration diode laser (λ = 785 and 830 nm) coupled (directly or by optical fiber) to a dispersive Raman spectrometer was employed to study two sets of human tissues (tooth and skin) in order to determine the set of experimental parameters suitable for luminescence rejection. It was concluded that systematic and reproducible spectra of biological interest can be acquired by SERDS.

©2010 Optical Society of America

OCIS codes: (170.0170) Medical optics and biotechnology; (170.4580) Optical diagnostics for medicine; (170.5660) Raman spectroscopy.

References and links

1. P. O. Andrade, R. A. Bitar, K. Yassoyama, H. Martinho, A. M. E. Santo, P. M. Bruno, and A. A. Martin, "Study of normal colorectal tissue by FT-Raman spectroscopy," Anal. Bioanal. Chem. **387**(5), 1643–1648 (2007).
2. R. A. Bitar, H. S. Martinho, C. J. Tierra-Criollo, L. N. Zambelli Ramalho, M. M. Netto, and A. A. Martin, "Biochemical analysis of human breast tissues using Fourier-transform Raman spectroscopy," J. Biomed. Opt. **11**(5), 054001 (2006).
3. C. Krishna, N. Prathima, R. Malini, B. Vadhiraja, R. Bhatt, D. Fernandes, P. Kushtagi, M. Vidyasagar, and V. Kartha, "Raman spectroscopy studies for diagnosis of cancers in human uterine cervix," Vib. Spectrosc. **41**(1), 136–141 (2006).
4. G. T. Webster, L. Tilley, S. Deed, D. McNaughton, and B. R. Wood, "Resonance Raman spectroscopy can detect structural changes in haemozoin (malaria pigment) following incubation with chloroquine in infected erythrocytes," FEBS Lett. **582**(7), 1087–1092 (2008).
5. A. Carden, and M. D. Morris, "Application of vibrational spectroscopy to the study of mineralized tissues (review)," J. Biomed. Opt. **5**(3), 259–268 (2000).
6. J. F. Ojeda, C. Xie, Y. Q. Li, F. E. Bertrand, J. Wiley, and T. J. McConnell, "Chromosomal analysis and identification based on optical tweezers and Raman spectroscopy," Opt. Express **14**(12), 5385–5393 (2006).
7. B. R. Wood, B. Tait, and D. McNaughton, "Micro-Raman characterisation of the R to T state transition of haemoglobin within a single living erythrocyte," Biochim. Biophys. Acta **1539**(1-2), 58–70 (2001).
8. C. Matthäus, B. Bird, M. Miljković, T. Chernenko, M. Romeo, and M. Diem, "Chapter 10: Infrared and Raman microscopy in cell biology," Methods Cell Biol. **89**, 275–308 (2008).
9. V. Pajcini, C. H. Munro, R. W. Bormett, R. E. Witkowski, and S. A. Asher, "UV Raman microspectroscopy: spectral and spatial selectivity with sensitivity and simplicity," Appl. Spectrosc. **51**(1), 81–86 (1997).
10. P. Mosier-Boss, S. Lieberman, and R. Newbery, "Fluorescence rejection in Raman spectroscopy by shifted-spectra, edge detection, and FFT filtering techniques," Appl. Spectrosc. **49**(5), 630–638 (1995).
11. E. V. Efremov, J. B. Buijs, C. Gooijer, and F. Ariese, "Fluorescence rejection in resonance Raman spectroscopy using a picosecond-gated intensified charge-coupled device camera," Appl. Spectrosc. **61**(6), 571–578 (2007).

#131531 - $15.00 USD Received 12 Jul 2010; revised 11 Aug 2010; accepted 13 Aug 2010; published 19 Aug 2010

12. A. Shreve, N. Cherepy, and R. Mathies, "Effective rejection of fluorescence interference in Raman spectroscopy using a shifted excitation difference technique," Appl. Spectrosc. **46**(4), 707–711 (1992).
13. B. D. Beier, and A. J. Berger, "Method for automated background subtraction from Raman spectra containing known contaminants," Analyst (Lond.) **134**(6), 1198–1202 (2009).
14. S. T. McCain, R. M. Willett, and D. J. Brady, "Multi-excitation Raman spectroscopy technique for fluorescence rejection," Opt. Express **16**(15), 10975–10991 (2008).
15. P. A. Mosier-Boss, S. H. Lieberman, and R. Newbery, "Fluorescence rejection in Raman spectroscopy by shifted-spectra, edge detection, and FFT filtering techniques," Appl. Spectrosc. **49**(5), 630–638 (1995).
16. D. Zhang, and D. Ben-Amotz, "Enhanced chemical classification of Raman images in the presence of strong fluorescence interference," Appl. Spectrosc. **54**(9), 1379–1383 (2000).
17. J. F. Brennan, Y. Wang, R. R. Dasari, and M. S. Feld, "Near-infrared Raman spectrometer systems for human tissue studies," Appl. Spectrosc. **51**(2), 201–208 (1997).
18. C. A. Lieber, and A. Mahadevan-Jansen, "Automated method for subtraction of fluorescence from biological Raman spectra," Appl. Spectrosc. **57**(11), 1363–1367 (2003).
19. J. Zhao, M. Carrabba, and F. Allen, "Automated fluorescence rejection using shifted excitation Raman difference spectroscopy," Appl. Spectrosc. **56**(7), 834–845 (2002).
20. S. E. J. Bell, E. S. O. Bourguignon, and A. Dennis, "Analysis of luminescent samples using subtracted shifted Raman spectroscopy," Analyst (Lond.) **123**(8), 1729–1734 (1998).
21. I. Osticioli, A. Zoppi, and E. M. Castellucci, "Shift-excitation Raman difference spectroscopy-difference deconvolution method for the luminescence background rejection from Raman spectra of solid samples," Appl. Spectrosc. **61**(8), 839–844 (2007).
22. L. E. S. Soares, E. B. P. S. Resende, A. Brugnera, Jr., F. A. A. Zanin, and A. A. Martin, "Combined FT-Raman and SEM studies of the effects of Er:YAG laser irradiation on dentin," Photomed. Laser Surg. **25**(4), 239–244 (2007).
23. B. Saleh, and M. Teich, Fundamentals of photonics, John Wiley & Sons, New York, 1991.

1. Introduction

In the last decade Raman Spectroscopy (RS) has become a very important tool for biological samples analysis, including cancer diagnosis [1–3], tropical disease diagnosis [4], dentistry [5] and cell studies [6–8]. RS offers certain advantages over others optical spectroscopic techniques, such as luminescence spectroscopy, polarized light scattering spectroscopy, optical coherence tomography and confocal reflectance microscopy. These advantages include high spatial (< 1 μm for micro-Raman setups) and spectral resolution (< 0.1 cm^{-1}), the possibility of using less harmful NIR radiation, less laborious preparation of samples (it is not necessary to introduce exogenous labels and in situ analysis could be performed), high chemical sensitivity, minimal influence of water bands, and the possibility of *in vitro* or *in vivo* data acquisition.

The spectroscopic instrumentation (detectors, gratings, lasers, etc.) and technology available have better performance in the visible spectral region (400-700 nm). However, Raman excitation in this range is not suitable for biological samples studies due to the strong auto-luminescence arising from samples. The strong luminescence signal masks the majority of Raman bands and decreases the signal to noise (S/N) ratio of the measurements affecting directly the sensitivity and specificity values. This limitation is one of the major obstacles to the wider use of RS for biological samples studies such as, e. g., medical optical diagnosis. One possible way to overcome this problem is to employ infrared (IR) radiation, specifically, Nd:YAG lasers at 1064 nm [1,2]. Reasonable S/N ratio spectra with this excitation are obtained only with the Fourier-Transform (FT) Raman technique, but due to the poor efficiency of CCD detectors in the infrared region, linear semiconductors detectors (InGaAs, Ge, etc) must be used. But in this case the 2D-multiplexing advantage of the dispersive setup is totally or partially lost. The FT technique demands high acquisition times (typically 1000 times more than dispersive techniques with poor spectral resolution) and sensitivity. Another option is employ ultraviolet (UV) radiation, where it is usually possible to obtain high quality spectra due to the elimination of luminescence and increase in the Raman intensity [9]. Nevertheless, the availability of UV instrumentation is limited, expensive, and can cause various types of damage to tissues, especially for *in vivo* applications.

Some methods have been developed in order to reduce luminescence and extract the vibrational information from the scattered Raman signal. Among them are polarization

#131531 - $15.00 USD Received 12 Jul 2010; revised 11 Aug 2010; accepted 13 Aug 2010; published 19 Aug 2010
(C) 2010 OSA

modulation [10], time-resolved picosecond excitation pulse and gating [11], shifted-excitation Raman difference spectroscopy (SERDS) [12], and computational algorithms for automated background subtraction [13–18].

Polarization modulation is based on the fact that the emitted luminescence does not conserve the polarization state of the exciting source. Thus, polarization sensitive detection will almost certainly eliminate the cross-polarized luminescence component of the Raman spectra. However, as the parallel-polarized fluorescence is normally non-negligible, this method has been ineffective in achieving this goal. Time-resolved Raman utilizes the fact that luminescence has a relatively longer life time (~10 −1000 ps) compared to Raman (~10 fs). Thus, by using pulsed lasers and limiting signal collection to just the time of the short pulse, can prevent the luminescence emission. This technique, however, involves sophisticated instrumentation and is not effective when the fluorescence lifetime is comparable to the excitation pulse duration [19]. Moreover, the spectral resolution decreases due to finite pulse of the laser. Shreve et al. [12] were the first to propose the SERDS method. It is based on fact that the luminescence spectrum is nearly insensitive to small energy excitation changes in contrast to that of the Raman bands. Thus, subtracting two Raman spectra, each one excited by slightly shifted laser lines could enable the elimination of the luminescence. Shreve et al. observed very good fluorescence removal using this method to measure the Raman spectra of a dye diluted in alcohol. A variation of this method was proposed by Mosier-Boss et al. [10]. In their proposal there was no shift of the excitation laser line, but a slight movement on the angle of the spectrometer diffraction grating to get two spatially shifted spectra. It was shown [19] that this is a poor method to remove the luminescence. Bel et al. [20] proposed a similar method of subtracting spectra taken at several different, closely spaced spectrometer positions excited with the same laser energy. The fluorescence-free Raman spectra were obtained by iterative fitting the bands to double Lorentzian functions. They obtained promising results using a dye in cyclohexane as the sample. However, it was pointed out that the main disadvantage of the method is the need for further complex data processing to obtain a recognizable Raman spectra [20]. Zhao et al. [19] and Osticioli et al. [21] used a mathematical method based on Fourier transform to automatically process the SERDS spectrum and obtain the pure Raman signal. The procedure applied to isopropanol [19], acetamide-phenol powder [19], cinnabar pigment [21] and sulphur [21] was reasonably successful to reconstruct the Raman bands. However, noise and spurious bands were observed. As pointed out by the authors the ability for good spectral reproduction strongly depends on the noise level in the raw spectra [21]. A similar limitation could be considered for the automated background subtraction [13–18] methods. In addition, it is desirable to develop a correct reconstruction procedure to know (have and/or measure) the spectra of the specific interfering fluorophore [13–18].

The aim of the present study was to make a systematic characterization and optimization of the experimental variables involved on a SERDS setup by testing the system in situations of biomedical interest (*in vitro* and *in vivo*). As far as we are concerned, similar applications of SERDS are not present in the literature.

2. Materials and methods

2.1 Raman Spectroscopy Instrumentation

Two optical setups for dispersive Raman experiments were employed for *in vitro* and *in vivo* macro-Raman applications. Figure 1 shows the schematic view of the SERDS system for macro-Raman measurements. A tunable Lithrow-configuration diode laser (λ = 785 or 830 nm – Sacher Lasertechnik) was used as the excitation source. The wavelength was mechanically adjusted using a home-made gear which enabled reproducible λ-shifts in 0.5 nm steps. For *in vitro* experiments [Fig. 1(a)], the laser was guided by optics and the Raman signal collected using a telescope. The laser spot diameter on the sample was 200 μm while typical acquisition

#131531 - $15.00 USD Received 12 Jul 2010; revised 11 Aug 2010; accepted 13 Aug 2010; published 19 Aug 2010
(C) 2010 OSA

time was 2 seconds. A notch filter (Semrock) was used to reject the Rayleigh scattering. The Raman signal was detected by a spectrometer (PiActon SpectraPro model 2500i) equipped with a N_2 cooled CCD detector (Princeton Instruments Spec-10). For *in vivo* applications it is desirable to take advantage of the remote probing characteristic of the optical fiber probes. The *in vivo* setup one [Fig. 1(b)] used an optical probe (EMVISION LLC) for both exciting the sample and collecting the Raman signal. In this case a laser at 785 nm was used as excitation source. To eliminate both the signals produced in the fibers and the elastically scattered light that enters into the collection fibers, a set of a long-pass and notch filter were glued on the distal side. The coupling between spectrometer and optical fiber was made using an SMA connector. In all cases the slit of the spectrometer was set to 100 μm. A home-made holder was employed to kept the proximal portion of the optical fiber 2 mm above the skin.

The tested parameters were: *(i)* the grating grooves (300, 600 and 1200 gr/mm) of the spectrometer holographic gratings; *(ii)* the laser line shifts $\Delta\lambda =$ 0.5; 1.5; 2.5 and 3.5 nm and *(iii)* laser excitation powers between 10 and 110 mW.

For comparative purposes, the FT-Raman spectra were also taken in each case. An FT-Raman spectrometer (Bruker RFS 100/S) with a Nd:YAG laser at 1064 nm as excitation source was used.

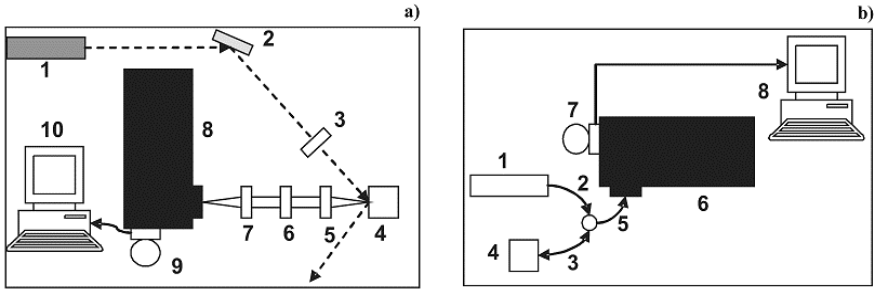

Fig. 1. (a) Schematic view of the SERDS system for macro-Raman *in vitro* measurements. (1) laser; (2) mirror; (3) convergent lens; (4) sample holder; (5) and (7) telescope; (6) notch filter; (8) spectrometer; (9) CCD camera; (10) computer. (b) Schematic view of the SERDS system for *in vivo* measurements. (1) laser; (2) optical probe laser-guide ; (3) optical probe excitation; (4) sample environment; (5) optical probe collecting; (6) spectrometer; (7) CCD camera; (8) computer.

2.2 Basic SERDS Theory

The total signal (S_R) measured when exciting a sample with light at wavelength λ is

$$S_R(\lambda) = \left[L(\lambda) + R(\lambda)\right] M(\lambda) + B(\lambda), \tag{1}$$

where $L(\lambda), R(\lambda), M(\lambda)$ and $B(\lambda)$ are the luminescence signal, Raman signal, optical response of the system, and background, respectively. For excitation at two slightly different wavelengths (λ_1 and λ_2) the above equation becomes:

$$S_R(\lambda_1) = \left[L(\lambda) + R(\lambda_1)\right] M(\lambda) + B(\lambda), \tag{2}$$

$$S_R(\lambda_2) = \left[L(\lambda) + R(\lambda_2)\right] M(\lambda) + B(\lambda), \tag{3}$$

since L, B and M are almost λ-independent.

The subtracted $\delta S \equiv S_R(\lambda_2) - S_R(\lambda_1)$ signal will have a derivative-like character for small wavelength shifts ($\Delta\lambda \sim$ linewidth of the typical Raman bands). It will be

#131531 - $15.00 USD Received 12 Jul 2010; revised 11 Aug 2010; accepted 13 Aug 2010; published 19 Aug 2010
(C) 2010 OSA

$$\delta S = \left[R(\lambda_2) - R(\lambda_1) \right] M(\lambda) \equiv \delta R(\lambda) M(\lambda) \quad (4)$$

which shows that δS is only related to the derivative-like Raman signal in this approximation.

The pure Raman signal could be recovered integrating Eq. (4):

$$R(\lambda) = \int M^{-1} \delta S d\lambda \quad (5)$$

where M^{-1} does not vary appreciably in the interval of interest for Raman measurements. Singularities, oscillatory, or fast decreasingly behavior of the quantum response of detectors or gratings could induce some artifacts when integrating the above expression. In our case, M was obtained by measuring the emission of a tungsten lamp and comparing it with the emissivity of a black-body at same temperature.

2.4 Samples

A non-carious third molar tooth was used to test the *in vitro* setup. It was sliced in a disc form with 4 mm of thickness and had been already characterized in a previous study [22]. The *in vivo* setup was tested on human skin of two voluntary students. They were informed about the objectives of the research as well as its ethical aspects and signed a consent form.

3. Results and discussion

3.1 In vitro Measurements

Figure 2 shows the Raman spectra of the human tooth taken with 300 [Fig. 2(a)]; 600 [Fig. 2(b)]; and 1200 [Fig. 2(c)] gr/mm with different excitation laser output powers ($P =$ 15, 45, 80, and 110 mW) at 830 nm. The light power delivered was almost the same since the absorption in the mirrors [Fig. 1(a)] is minimal. All spectra were processed in order to have the most intense (low Raman shift) point normalized to one after subtracting the intensity of the higher wavenumber experimental point. Thus, all spectra were normalized to 0 - 1. This is a good way to standardize the background (luminescence) contribution. Those spectra taken at 15 mW (50 mA) appeared less intense compared to the luminescence than the other ones. In fact this power is close to the lasing current threshold ($\sim$ 40 mA) and there is significant contamination by non-laser light impinging the sample. The prominent band at 950 cm^{-1} is the PO_4^- vibration of hydroxy-apatite [22]. The spectral windows/resolutions were 1850/1.6; 960/0.8; 420/0.3 cm^{-1} for 300; 600; and 1200 gr/mm gratings, respectively. The 300 gr/mm [Fig. 2(a)] grating presented the most intense peaks, with the largest spectral window, but with the smallest spectral resolution when compared to the others. The 1200 gr/mm grating [Fig. 2(b)] presented the best spectral resolution but less intense peaks and the smallest spectral window. The 600 gr/mm grating presented intermediate characteristics between those obtained with the 300 and the 1200 gr/mm gratings.

#131531 - $15.00 USD Received 12 Jul 2010; revised 11 Aug 2010; accepted 13 Aug 2010; published 19 Aug 2010
(C) 2010 OSA

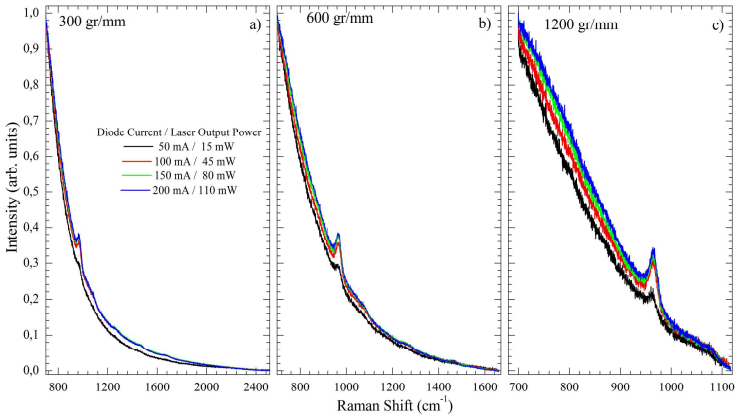

Fig. 2. (Color online) Raman spectrum of a human tooth with 300 (a); 600 (b); and 1200 (c) gr/mm gratings in function of outputs power 15, 45, 80 and 110 mW.

The spectral differences δS are shown on Fig. 3 for several conditions. In order to have the Raman bands comparable a second normalization procedure was need where the subtracted spectra were normalized to the maximum intensity. Panels I, II, and III show the spectra obtained with 300, 600, and 1200 gr/mm gratings, respectively. The powers employed were $P = 15$ mW (a), 45 mW (b), 80 mW (c), and 110 mW (*d*) and $\Delta\lambda =$ 0.5; 1.5; 2.5, and 3.5 nm. With $P < 15$ mW [Fig. 3(a) Panels I-III] the height of the derivative-like Raman band at 960 cm^{-1} was less than two times the noise level. This ratio is greater than 10 for other power levels. The signal to noise ratio (S/N) became constant ($\sim$ 0.013) at $P =$ 80 mW [Fig. 3(c)] for all gratings. This indicates that better spectra were acquired with $P > 80$ mW. It was found that higher $\Delta\lambda$ distorted the linear form of the inflection signal. For example, for 300, 600, and 1200 gr/mm gratings this distortion started at $\Delta\lambda =$ 3.5; 2.5; and 1.5 nm, respectively.

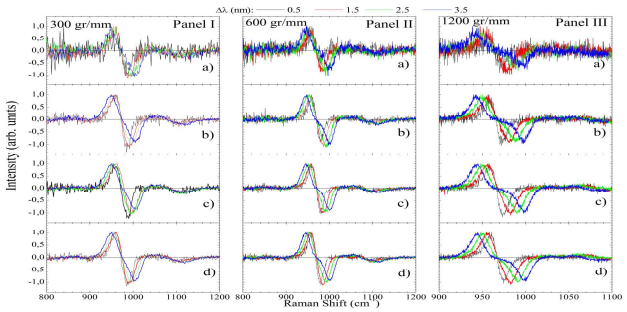

Fig. 3. (Color online) δS for a human tooth obtained with 300 (Panel I); 600 (Panel II); and 1200 (Panel III) gr/mm gratings. Different output powers (15 (a); 45(b); 80(c); and 110 (d) mW) and wavelength displacements ($\Delta\lambda = 0.5$; 1.5; 2.5; and 3.5 nm) from the principal laser line were tested.

Figure 4 shows the inverse of the optical response $M^{-1}(\lambda)$ for the 300 (a), 600 (b), and 1200 (c) gr/mm gratings normalized to 0-1 to better comparison. The 300 gr/mm [Fig. 4(a)] grating presented a very flat signal between 1000 and 2200 cm^{-1}. The 600 gr/mm grating showed a quite smooth behavior between 780 and 1450 cm^{-1} while presenting nonlinearities at the borders. The 1200 gr/mm grating showed an exponentially decreasing response modulated by several noisy bumps and peaks.

#131531 - $15.00 USD Received 12 Jul 2010; revised 11 Aug 2010; accepted 13 Aug 2010; published 19 Aug 2010
(C) 2010 OSA

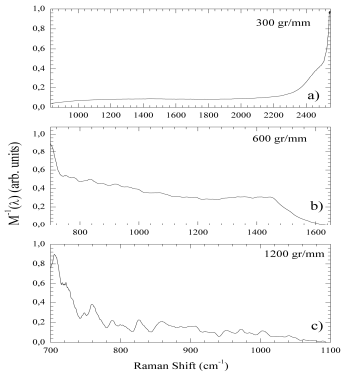

Fig. 4. (Color online) The inverse of the optical response (M^{-1}) normalized to 0-1 for 300 (a); 600 (b); and 1200 (c) gr/mm gratings.

The integrated spectra of Fig. 3 after correction to M^{-1} and subsequent normalization to 0-1 are shown in Fig. 5. At first glance it is clear that there is a broadening effect at higher $\Delta\lambda$ s. It was observed bands at 800; 871; 882; 961; 1040; and 1071 cm^{-1} for the 300 gr/mm grating with $\Delta\lambda =$ 0.5 nm [Fig. 5(a)]. As the expected bands would be at 816; 856; 880; 961; 1005; 1030; 1045; and 1071 cm^{-1} [22], those seen at 800 and 871 cm^{-1} were spurious signal. Moreover, the expected bands at 816; 856; 1005; 1030 cm^{-1} were not observed. Increasing the λ-shift to $\Delta\lambda = 1.5$ nm the band at 800 cm^{-1} disappeared; those at 871 and 882 cm^{-1} superimposed into a single band at 867 cm^{-1}; the band at 961 cm^{-1} shifted to 966 cm^{-1} while an increasing broadening occurred; and those at 1040 and 1071 cm^{-1} collapsed into a broad band centered at 1075 cm^{-1}. These spectral features were broadened for $\Delta\lambda = 2.5$ and 3.5 nm. An additional band at 1060 cm^{-1} was seen in the $\Delta\lambda = 3.5$ nm spectra.

Figure 5(b) presents the data for the 600 gr/mm grating. For $\Delta\lambda = 0.5$ nm bands at 816; 823; 856; 880; 961; 1045; and 1071 cm^{-1} were observed. Those at 1045 and 1071 cm^{-1} were more resolved than in the previous case while just one spurious band at 823 cm^{-1} was observed. Similar artifacts were observed in Fig. 5(a) with $\Delta\lambda = 1.5 - 3.5$ nm for the 600 gr/mm grating. Figure 5(c) shows the spectra for the 1200 gr/mm grating. Above the noise level the 914; 850; 880; 961 and 1081 cm^{-1} bands were observed for $\Delta\lambda =$ 0.5 nm. Only two bands (880 and 961 cm^{-1}) correspond to the expected ones. For $\Delta\lambda = 1.5$ nm, the 1081 cm^{-1} band shifted to 1084 cm^{-1}. Its frequency decreases to 1065 cm^{-1} for $\Delta\lambda = 2.5$ and 3.5 nm.

#131531 - $15.00 USD Received 12 Jul 2010; revised 11 Aug 2010; accepted 13 Aug 2010; published 19 Aug 2010
(C) 2010 OSA

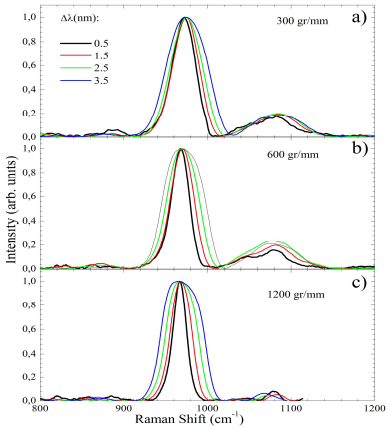

Fig. 5. (Color online) SERDS spectrum of human tooth for the 300 (a); 600 (b); and 1200 (c) gr/mm gratings and $\Delta\lambda =$ 0.5; 1.5; 2.5 and 3.5 nm.

Another important parameter to discuss is the root mean square signal to noise ratio (*S/N*(*RMS*)). For comparison we will discuss the S/N ratio only for $\Delta\lambda =$ 0.5 nm data. *S/N*(*RMS*) = 0.373; 0.434; and 0.371 for 300, 600, and 1200 gr/mm were observed, respectively. Thus, the best S/N ratio was found with the 600 gr/mm grating. It also had good spectral resolution (0.8 cm^{-1}) while displaying spectral window width ~960 cm^{-1} and relatively smooth behavior between 780 and 1450 cm^{-1}. Nevertheless, it was concluded that the best set of parameters was $\Delta\lambda =$ 0.5 nm and the 600 gr/mm grating. It is worth to notice the relevant improvement in the S/N ratio compared to the raw data (Fig. 2). As pointed out by previous work [19], this is due to the fixed pattern noise elimination and the double integration time associated to the two spectra acquisition. However, the random white noise (shot noise) cannot be removed with this technique.

Figure 6 shows the SERDS spectra for human tooth using the best set of parameters ($\Delta\lambda =$ 0.5 nm; 600 gr/mm; 110 mW) and following the same steps presented earlier to acquire the pure Raman signal. Figure 6(a) displays the two shifted spectra while Fig. 6(b) and 6(c) shows the subtracted signal and the integrated one, respectively. The fluorescence removal is evident when comparing Figs. 6(a) and 6(c). In Fig. 6(c) the FT-Raman spectra of the same tooth is presented. The spectra were almost identical.

3.2 In vivo Measurements

Figure 7 shows the SERDS procedure to take human skin spectra with an optical fiber probe. This procedure was employed in a similar analysis of *in vitro* case and it was concluded that the best set of parameters were $\Delta\lambda = 0.5$ nm; 600 gr/mm grating; and 70 mW laser power.

Figures 7(a), 7(b) and 7(c) displays the two shifted spectra (in wavelength units), the subtracted signal, and the integrated one, respectively. The SERDS and FT-Raman spectra are compared in Fig. 7(c). The overall spectral features are present in the SERDS spectra. However, some relevant differences could be identified when subtracting FT-Raman and SERDS spectra [Fig. 7(d)]. The bands between 750 and 1200 cm^{-1} appeared less intense in the SERDS spectra when compared to the FT-Raman one. Otherwise, the bands in the 1200-1580 cm^{-1} region appeared more intense in the SERDS spectra.

#131531 - $15.00 USD Received 12 Jul 2010; revised 11 Aug 2010; accepted 13 Aug 2010; published 19 Aug 2010
(C) 2010 OSA

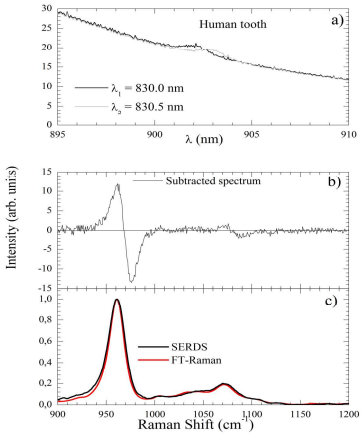

Fig. 6. (Color online) (a) Two spectra obtained for a human tooth at λ_1 = 830.0 nm and λ_2 = 830.5 nm. (b) Subtracted spectrum (δS). (c) SERDS spectrum compared to the FT-Raman one.

We argue that the main cause of these differences relies on the etaloning effect that occurs on back-illuminated CCD detectors working in the near infrared region. Coating of the CCD surface with anti-reflecting material could minimize this effect but does not completely suppress it. Reflections between parallel front and back surfaces cause the CCD to act as a partial etalon. The effect is an oscillatory modulation of the detected signal. The two arrows on Fig. 7(a) indicate two bands probably due to the etaloning modulation. The three factors that determine the shape and intensity of the etaloning effect are the thickness of the CCD, *d*, the wavelength of the light, λ, and the light absorption by the CCD material expressed as the finesse constant, *Q* [23]. The resulting etaloning intensity will follows the equation [23]

$$E(\lambda) = \frac{I_{\max}}{1 + \left(\frac{2Q}{\pi}\right)^2 \sin^2\left(\frac{2\pi d}{\lambda}\right)} \tag{6}$$

Thus, the total signal in Eq. (1) needs to be modified to

$$S_R(\lambda) = \left[L(\lambda) + R(\lambda)\right] M(\lambda) E(\lambda) + B(\lambda).$$

As just stated before, for a very close wavelength shift one could consider *L* and *M* as λ-independent. As a consequence the M^{-1}-corrected differential of S_R will be

$$M^{-1} dS_R = R(\lambda) \frac{dE}{d\lambda} d\lambda + E(\lambda) \frac{dR}{d\lambda} d\lambda \tag{7}$$

and to completely recover the pure Raman signal $R(\lambda)$ one will need to solve this differential equation. As a first approximation one could also consider *E* almost constant and the derivative of $E(\lambda)$ respect to λ as zero. Thus, Eq. (7) simplifies to

$$M^{-1} dS_R = E(\lambda) \frac{dR}{d\lambda} d\lambda$$

and Eq. (5) will be re-written as

$$R(\lambda) = \frac{1}{E} \int M^{-1} \delta S d\lambda \tag{8}$$

#131531 - $15.00 USD Received 12 Jul 2010; revised 11 Aug 2010; accepted 13 Aug 2010; published 19 Aug 2010
(C) 2010 OSA

which requires one to consider the etaloning effect as a correction factor after the integration of the subtracted signal. The etaloning parameters in our case were estimated by analyzing the subtracted FT-Raman and SERDS signal [Fig. 7(d)]. It is clear that the modulation of the overall signal by an envelope is due to the oscillatory function. The fitting of the signal envelope is shown as a dashed line on Fig. 7(d). The obtained parameters were I_{max} = 1.33; Q = 1.31; and d = 4 nm.

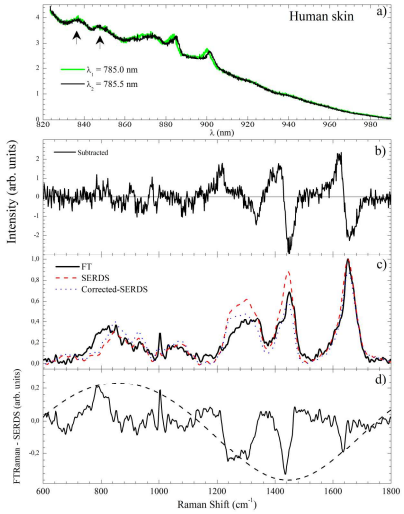

Fig. 7. (Color online) (a) Two human skin spectra obtained at λ_1 = 785.0 nm and λ_2 = 785.5 nm. (b) Subtracted spectrum. (c) FT-Raman (solid line), SERDS (dashed line) and corrected-SERDS (dotted line) spectra. (d) SERDS subtracted FT-Raman spectra. The dashed line is a fitting to Eq. (6) as discussed in text.

The dashed line in Fig. 7(c) is the SERDS spectra corrected by the above-estimated etaloning signal. It could be observed that the relative intensities were more realistic when compared to the FT-Raman signal. However differences still persist and we argue that they will be fixed once $R(\lambda)$ is obtained directly from Eq. (7) without approximations. Numerically solving this equation is a complex procedure and is beyond the scope of the present work.

4. Conclusions

Our results indicated that the SERDS method could be used to eliminate undesired luminescence background in a very systematic and reproducible way. A successful background removal from different kinds of human biological tissues as tooth and skin has been reported. It was found that each sample had a specific set of parameters (grooving of the grating, laser power, and $\Delta\lambda$) that maximizes the luminescence elimination and minimizes the spectra distortion. It was found that $\Delta\lambda = 0.5$ cm^{-1} is the best wavelength variation in all experiments. The grating and laser power depend on the specific case. The etaloning effect could represent an important source of interference mainly when the overall scattered signal is high (as in the human skin case). One way to overcome this problem is to perform a preliminary characterization of the etaloning signal present in the detector conjugated to some previous knowledge about the expected Raman bands.

Acknowledgments

The authors would like to thank Karl J. Jalkanen for the critical reading of the manuscript and the CNPq, CAPES, and FAPESP Brazilian agencies for the financial support.

#131531 - $15.00 USD Received 12 Jul 2010; revised 11 Aug 2010; accepted 13 Aug 2010; published 19 Aug 2010
(C) 2010 OSA